Atmos. Meas. Tech. Discuss., 7, 5147–5172, 2014
www.atmos-meas-tech-discuss.net/7/5147/2014/
doi:10.5194/amtd-7-5147-2014
© Author(s) 2014. CC Attribution 3.0 License.

Atmospheric Measurement Techniques Discussions

This discussion paper is/has been under review for the journal Atmospheric Measurement Techniques (AMT). Please refer to the corresponding final paper in AMT if available.

Impact of the aerosol type on HICO™ atmospheric correction in coastal waters

C. Bassani[1], C. Manzo[1], F. Braga[2], M. Bresciani[3], C. Giardino[3], and L. Alberotanza[2]

[1]Institute for Atmospheric Pollution Research (IIA), Italian National Research Council (CNR), Via Research Area of Rome 1, Via Salaria Km 29,300, 00016 Monterotondo Scalo, Rome, Italy
[2]Institute of Marine Sciences (ISMAR), Italian National Research Council (CNR), Arsenale Tesa 104, Castello 2737/F, 30123 Venice, Italy
[3]Institute for Electromagnetic Sensing of the Environment (IREA), Italian National Research Council (CNR), Via Bassini 13, 20133 Milan, Italy

Received: 6 February 2014 – Accepted: 13 May 2014 – Published: 23 May 2014

Correspondence to: C. Bassani (cristiana.bassani@iia.cnr.it)

Published by Copernicus Publications on behalf of the European Geosciences Union.

Abstract

The aim of this work is to evaluate the radiative impact of the aerosol type on the results of the atmospheric correction of HICO™ (Hyperspectral Imager for the Coastal Ocean) hyperspectral data. The reflectance was obtained by using the HICO@CRI (HICO ATmospherically Corrected Reflectance Imagery) algorithm, a physically-based atmospheric correction algorithm developed specifically for HICO™ data by adapting the vector version of the Second Simulation of a Satellite Signal in the Solar Spectrum (6SV) radiative transfer code. The HICO@CRI algorithm was applied on six HICO™ images acquired in the Northern part of the Mediterranean Basin, using the micro-physical properties measured with a CIMEL sun sky-radiometer at the Acqua Alta Oceanographic Tower (AAOT) AERONET site and the optical properties of the maritime, continental, and urban aerosol types provided by default by the 6SV. The results highlight that the aerosol type can improve the accuracy of the atmospheric correction. Indeed, the accuracy of the water reflectance retrieved from the available HICO™ data decreases in the sensor spectral domain, considering the AERONET micro-physical properties, of 30 % using the urban aerosol type, of 20 % using the continental type, and finally of less than 10 % assuming a maritime type. Thus, the aerosol type has to be taken into consideration in the atmospheric correction of hyperspectral data over coastal environment, if water quality analysis has to be performed, because of the influence of aerosol type on the water reflectance.

1 Introduction

The radiative impact of aerosol is a key issue in the atmospheric radiative transfer models devoted to the earth/atmosphere coupled system (Kokhanovsky, 2008). Great efforts have been made to study the aerosol from remote sensing data as presented in Kaufman et al. (1997b, a); Holben et al. (1998); King et al. (1999); Levy et al. (2007); Kokhanovsky et al. (2007, 2010); Bassani et al. (2010). These studies

AMTD
7, 5147–5172, 2014

have demonstrated the crucial role of the aerosol optical thickness at 550 nm, τ_{550}, in the atmospheric radiative transfer modeling. Several studies (Kotchenova et al., 2008; Vermote et al., 1997b; Kaufman et al., 2002; Guanter et al., 2007, 2009b; Gao et al., 2009; Goetz et al., 1985) showed the role of τ_{550} on the atmospheric correction of multi- and hyperspectral data dedicated to the retrieval of ocean and land properties. A series of physically-based algorithms to retrieve aerosol loading (τ_{550}) from remote sensing images have been developed, using MODIS both over land (Kaufman et al., 1997a) over ocean (Tanré et al., 1997) and using the hyperspectral CHRIS-PROBA sensor (Guanter et al., 2005). However, neither the variability of aerosol type nor the possible influence of this variability on the atmospheric correction results is evaluated.

In this context, the focus of this work is to evaluate the impact of aerosol type on the results of the atmospheric correction of the HICO™ (Hyperspectral Imager for the Coastal Ocean) data acquired in a coastal environment in the northern Adriatic Sea. In a previous study, (Bassani et al., 2012), the aerosol type was connected to the accuracy of aerosol loading for the reflectance retrieval from hyperspectral spaceborne data. In this study a new algorithm, HICO@CRI (HICO™ ATmospherically Corrected Reflectance Imagery), was developed to perform the atmospheric correction of HICO™ data. The HICO@CRI is based on the vector version of the Second Simulation of a Satellite Signal in the Solar spectrum (6SV) atmospheric radiative transfer code (Vermote et al., 2006), which is the improved open-source code of the 6S (Vermote et al., 1997b) used for the new generation atmospheric correction algorithm of MODIS data (Vermote and Kotchenova, 2008).

The water reflectance was obtained by running the HICO@CRI algorithm with maritime, continental, and urban aerosol types provided by default by 6SV. An additional run was performed using the micro-physical properties of the aerosol provided by the Acqua Alta Oceanographic Tower (AAOT) station (Mélin et al., 2006) of the widespread AERONET network (Holben et al., 1998). Results from last run allow to build a reference, against which the output obtained by running HICO@CRI with the three 6SV default aerosol types can be compared. The NRMSE (Normalized Root Mean Square)

AMTD
7, 5147–5172, 2014

was used to evaluate the radiative impact of 6SV default aerosol types with respect to the AERONET inversion products.

2 Site

The Acqua Alta Oceanographic Tower (AAOT) is located in the northern part of the Adriatic Sea, 15 km off the Venice lagoon (12.51° E, 45.31° N). The AAOT (Mélin et al., 2006) is an automated station of the spreadworld AERONET network (Holben et al., 1998). Besides atmospheric acquisitions, the CIMEL sun sky-radiometer instrument at AAOT also performs ocean color measurements for the AERONET-OC network (Zibordi et al., 2009).

The site is in a coastal area generally affected by continental or urban aerosol, as reported in Mélin et al. (2006). Neverthless, since it is located in the Mediterranean Sea, the possible presence of maritime aerosol was also taken into account.

3 Data

The data used in this study were acquired by using two passive remote sensing instruments operating in the visible spectral domain. The atmospheric data were obtained from the in situ automatic tracking sun sky-radiometer CIMEL CE-318 of the AAOT station (Holben et al., 1998; Smirnov et al., 2011, 2009; Mélin et al., 2006), while image data come from the HICO™ hyperspectral sensor (Lucke et al., 2011).

The CIMEL CE-318 provides the aerosol optical thickness at the nominal wavelengths (440, 500, 670, 870, 940, 1020 nm), the columnar content of water vapor, wvcc, and ozone, occ, by measuring the direct component of the solar irradiance. From the measurements of the diffuse component on four bands (442, 668, 870, 1020 nm) of the sky radiance at specific angles, the AERONET inversion products, aerosol microphysical and optical properties, are retrieved.

AMTD
7, 5147–5172, 2014

The atmospheric data have three quality levels: level 1.0 (unscreened), level 1.5 (cloud-screened), and level 2.0 (cloud-screened and quality-assured). The lev 2.0 of atmospheric properties is used for atmospheric correction, and also the level 1.5 has been largely used for remote sensing applications, principally the micro-physical properties being often limited to lev 1.5.

The HICO™ sensor (Lucke et al., 2011), is the first spaceborne hyperspectral sensor dedicated to the coastal and inland monitoring and ocean characterization. The sensor is composed of 87 contiguous channels in the spectral domain 400–900 nm with a the Full Width at Half Maximum (FWHM) of about 10 nm. The ground swath is about 43.5 km with pixel size of 87 m at nadir acquisition, becoming 93 km with 182 m pixel size at 45° for the view zenith angle. The signal-to-noise ratio (SNR) is > 200 : 1 over 400–600 nm as reported in Lucke et al. (2011).

Table 1 shows the six HICO™ images with corresponding AAOT data to constrain the τ_{550}, the wvcc, and the occ. The Angstrom coefficient has been also reported for the qualitative evaluation of the aerosol size from the measurements of direct solar irradiance. In order to analyze the contribution of the aerosol type on the water reflectance obtained by using the HICO@CRI algorithm, the AERONET inversion products (micro-physical properties) of the AAOT AERONET station and three aerosol types (maritime, continental and urban) were considered for the atmospheric correction.

Figure 1 shows the micro-physical properties, size distribution, and the real and imaginary part of the refractive index retrieved from the diffuse measurements of solar radiance by using the CIMEL CE-318. In the left plot, the bimodal distribution of the aerosol size is in agreement with the results reported in Mélin et al. (2006), except for the 25 April 2013 where the accumulation mode prevails in the volume size distribution. The 4 May 2011 presents a tri-modal size distribution, observed for low aerosol loading in the site (Mélin et al., 2006). The other plots show the real and imaginary parts of the refractive index. The spectral values of the imaginary part attest non negligible absorption of aerosol in the coastal area during data acquisition, especially on 11 January 2012, while observations on 4 May 2011 underlines the presence of

AMTD
7, 5147–5172, 2014

non-absorbing particles in the atmosphere. The micro-physical properties, size distribution and refractive index, permit detailed evaluation of the aerosol impact on the atmospheric correction of HICO™ data. The aerosol optical properties required for radiative modeling and used for the atmospheric correction, were derived from these micro-physical properties by using the subroutines MIE and AEROSOL included in the 6SV source code (Vermote et al., 2006).

The 6SV default aerosol types (cf. Sect. 2) are defined according to a combination of the four basic components: sea-salt, water-soluble, soot and dust-like (Lenoble, 1985; d'Almeida et al., 1991; Kokhanovsky, 2008; Vermote et al., 2006). Table 2 shows the volumetric percentage of the basic components for the three aerosol types. Figure 2 shows the single-scattering albedo (left) and the asymmetry parameter (right) of the three 6SV default aerosol types and of the measurement days. In Fig. 2 the continous lines represent the optical properties simulated by the MIE and AEROSOL subroutines of 6SV while the dots indicate the corresponding values obtained by the CIMEL measurements. Simulated and measured data are indicated with the same color for each day (cf. Table 1).

It is evident from Fig. 2, the AERONET inversion products are comparable to the spectral behaviour of maritime type, in contrast with the dominating influence of continental and anthropogenic aerosol reported in Mélin et al. (2006).

4 Methods

The methodology applied in this work is based on the analysis of the contribution of the aerosol type on the water reflectance to improve the accuracy of sea surface reflectance, whose assessment is closely related to the retrieval of water quality parameters (chlorophyll, total suspended matter and colored dissolved organic matter), (Zibordi et al., 2011; Giardino et al., 2010; Guanter et al., 2010; Brando and Dekker, 2003). The physically-based atmospheric correction algorithm, HICO@CRI, which relies on the 6SV code, was developed to accept wvcc, occ, τ_{550} and type of the aerosol.

AMTD
7, 5147–5172, 2014

Concerning the aerosol type, the AERONET inversion products (i.e. the micro-physical properties of the aerosol) or the default aerosol types (i.e. percent of the basic components) can be introduced in the algorithm.

The algorithm for the atmospheric correction of HICO™ image was implemented in the open source GDL programming language (Coulais et al., 2009; Arabas et al., 2010), following the method reported in Bassani et al. (2010). Starting from the at-sensor radiance, L_v, the equation presented in Vermote et al. (1997b) was used under the assumption of isotropy surface (Lambertian surface), to neglect the influence of the solar and viewing angles on the surface reflectance, such as the Bi-directional Reflectance Distribution Function (BRDF) of the surface. Thus, the results of HICO@CRI application can be addressed to the aerosol type without contribution of the geometrical conditions to the retrieved surface reflectance.

The equation solved for the surface reflectance (Bassani et al., 2010) for each HICO™ channel, ρ_{gnd}, is the following:

$$\rho_{gnd} = \frac{t_g\rho_{atm} - \rho_{TOA}}{S(t_g\rho_{atm} - \rho_{TOA}) - t_S t_g} \quad (1)$$

where $\rho_{TOA} = \pi L_v/\mu_s E_s$ is the sensor reflectance expressed by the TOA (Top Of Atmosphere) solar irradiance, E_s, and by the cosine of the solar zenith angle, $\mu_s = \cos(\theta_s)$. The residual variables are radiative quantities simulated with a spectral sampling of 2.5 nm covering the domain from 400 nm to 900 nm by using the last version, 6SV, (Kotchenova et al., 2008) of the Second Simulation of a Satellite Signal in the Solar Spectrum, 6S, (Vermote et al., 1997b) radiative transfer code. t_g is the gas transmittance; ρ_{atm} is the atmospheric reflectance, called path radiance. S is the atmospheric spherical albedo, (Kokhanovsky, 2008). $t_S = t^{\uparrow} + t^{\downarrow}$ is the total transmittance, obtained from the downward and upward direction. Each one is composed by the direct and diffuse component, $t^{\uparrow,\downarrow} = e^{-\tau(\lambda)/\mu_{v,s}} + t^{\uparrow,\downarrow}_{dif}$. $\mu_{v,s} = \cos(\theta_{v,s})$ are the cosine of the view (v) and sun (s) zenith angles and τ is the total optical thickness due to the aerosol and gases.

AMTD
7, 5147–5172, 2014

The HICO@CRI algorithm computes the convolution of the radiative quantities, simulated with 2.5 nm spectral sampling, on the spectral response of HICO™ sensor assumed gaussian with the central wavelength and the FWHM allowed in the header file of the image; procedure is described in Bassani et al. (2010).

The geolocated and geometric input are loaded in the HICO@CRI algorithm from a file supplied with each HICO™ image, where the following data are contained: longitude (degrees), latitude (degrees), the viewing zenith (VZA) and azimuth (VAA) angles, and the solar zenith (SZA) and azimuth (SAA) angles, referred to each pixel of the image. These values permit to simulate the radiative quantities for each pixel avoiding errors for the calculation of the geometrical configuration of the acquisition.

The surface reflectance, $\rho(\lambda)$, is finally retrieved removing the effect of the neighboring pixels to the pixel viewing from the sensor, by using the empirical formula employed in atmospheric correction algorithms (Bassani et al., 2010; Guanter et al., 2007, 2009a; Kotchenova et al., 2008; Vermote et al., 1997b, a)

$$\rho(\lambda) = \rho_{\mathrm{gnd}} + \frac{t_{\mathrm{dif}}^{\uparrow}}{e^{-\tau(\lambda)/\mu_{\mathrm{v}}}}[\rho_{\mathrm{gnd}} - \langle\rho_{\mathrm{gnd}}\rangle] \quad (2)$$

In Eq. (2) $\langle\rho_{\mathrm{gnd}}\rangle$ is the mean of the pixels adjacent to the viewing pixel covering the swath of the HICO™ sensor, approximately 30 km^2. This is the empirical approximation of the environmental contribution to the radiance reaching an airborne or spaceborne sensor.

Concerning the atmospheric input, the HICO@CRI algorithm loads parameters of aerosol and gases. Evaluation of the role of aerosol type on the results of the atmospheric correction over coastal area needs an accurate aerosol loading, by the τ_{550}, and the columnar content of the gas with the absorption bands falling into sensor channels. At present, the considered gas parameters are the columnar content of water vapor, wvcc, and ozone, occ. The known and constrained properties related to the gas and to the aerosol loading guarantee that the variability of the atmospheric correction results is only due to the aerosol type.

AMTD
7, 5147–5172, 2014

In the HICO@CRI algorithm, τ_{550} can be varied as well as the aerosol size distribution and the refractive index (if CIMEL CE-318 data have to be used) or the volumetric percentage of the basic components (if default 6SV aerosol types are used).

The aerosol loading is a primary characteristic for the atmospheric radiative transfer applied to the remote sensing data. The optical parameter of aerosol acknowledged to describe the aerosol loading (Kaufman et al., 1997a) is the aerosol optical thickness at 550 nm, τ_{550}. Other aerosol optical properties relevant to atmospheric radiative transfer modeling are defined by the aerosol type. Consequently, the radiative quantities of the Eqs. (1) and (2) are expected to depend on aerosol type and thus the results of the atmospheric correction, water reflectance, should be different.

The micro-physical properties, downloaded from the AAOT station and used as input in the HICO@CRI, are the size distribution and the refractive index (cf. Fig. 1). Otherwise, in the developed algorithm, aerosol types can be introduced from the 6SV default types defined by the optical properties (Vermote et al., 2006), described in the Sect. 3.

5 Results

The HICO™ images, reported in Table 1, were processed by applying HICO@CRI algorithm. The geolocated and geometric inputs were taken from the ancillary data; the atmospheric inputs (τ_{550}, wvcc, and occ) were constrained by the AERONET products, while the parameters defining the type of aerosol were varied. In the first step, the atmospheric correction was performed considering the micro-physical properties of the aerosol provided by AAOT site; in the second step, considering the optical properties of the three 6SV default aerosol types (continental, maritime, and urban). Thus, for each HICO™ image, four corrected images were obtained.

The differences among the retrieved products are analyzed for different water types observed in each HICO image. To this end, three Regions Of Interest (ROIs) were selected on the basis of the variability and representativity of the water surface relatively to each HICO™ image (cf. Table 1). The Euclidean Distance (ED) between the sensor

AMTD
7, 5147–5172, 2014

radiance in correspondence of the maximum, 550 nm, and the minimum, 680 nm, of the solar radiation reaching the sensor coming from target of water was used. The radiance measured by the sensor was considered to classify the water surface independently from the atmospheric correction procedure. The locations of the ROIs were defined with similar geometrical configuration to neglect different radiative contribution on the sensor radiance, due to the viewing and illumination angles between the ROIs of each image. Besides, the ROIs were selected close to the AAOT station in order to avoid the impact of horizontal atmospheric variability within the HICO™ scenes.

Figure 3 shows the ROIs chosen for each HICO™ image used in this study. The red ROI (ROIrL) is representative of water with low luminosity in the image, the blue and green ROIs represent water with medium (ROIbM), and high (ROIgH) luminosity, respectively. For each HICO™ image, four mean reflectance values were calculated with respect to the three ROIs obtained for the three 6SV default aerosol types and for the AERONET inversion products.

Figure 4 shows the average of the water reflectance retrieved by using the AERONET inversion products calculated for each ROI (cf. Fig. 3) and used as benchmark for the evaluation of the radiative impact of the aerosol type on the atmospheric correction processing. The retrieval of the water reflectance was performed for high (ROIgH), medium (ROIbM), and low (ROIrL) reflectance of the water. The noisy reflectance can be attributed to the effect of the signal-to-noise (SNR) ratio of HICO™ sensor calculated for low reflectance cases, as reported by Moses et al. (2012). The negative values of reflectance obtained from correction of the HICO™ image acquired the 12 May 2012 is explained by the limits of accuracy of the radiative transfer simulation for early morning irradiance case as shown in Table 1. Besides, the negative values of reflectance on 4 May 2011 could be likely due to the loos of accuracy of the simulation results produced by the tri-modal size distribution obtained from CIMEL measurements, as shown in Fig. 1.

Figure 5 shows the ED between the reflectance retrieved using the AERONET inversion products and the 6SV default aerosol types (maritime, continental, and urban).

AMTD
7, 5147–5172, 2014

The ED is reported for the HICO™ channels centered in atmospheric windows, to point out the aerosol radiative impact avoiding the gas influence during the extinction modelling. Panels on the left show the ED for the image with the minimum of the τ_{550} = 0.01 and panels on the right shows the results for the maximum, τ_{550} = 0.27.

In order to quantify the contribution of each 6SV default aerosol type on the spectral water reflectance with respect to the AERONET inversion products, the Root Mean Square Error (RMSE) was normalized to the distance between the outer limits (maximum and minimum) of each spectral water reflectance.

Figure 6 shows the Normalized Root Mean Square Error (NRMSE) vs. the τ_{550} for the three ROIs, where the water reflectance accuracy decreases with growing aerosol loading, particularly when an unsuitable aerosol type is selected. The aerosol loading changes slowly the accuracy of atmospheric correction results if an aerosol type, having similar optical properties of the AERONET inversion products, is considered. In the case study, the aerosol type which better satisfies the condition is the maritime one, while, if a continental aerosol is assumed, the accuracy decreases less if urban is selected.

During acquisition periods, aerosol was mainly distribuited in the fine mode, showing a non negligible imaginary part of refractive index, with the exception of 4 May 2011 and 25 April 2013. The NRMSE for the 4 May 2011 is higher than for the other ones (Fig. 6). The imaginary part of the refractive index is negligible only for the aerosol type during the HICO™ acquisition of the 4 May 2011, as shown in Fig. 1. Thus, the radiative impact of aerosol absorption plays a crucial role on the atmospheric correction of hyperspectral data over water target in coastal environment. On the other hand, the Fig. 1 shows a size distribution of the 25 April 2013 with a predominance in coarse mode. The aerosol size affects weakly the accuracy of the retrieved water reflectance, as shown in Fig. 6 in the case study of 25 April 2013 defined with high aerosol loading, τ_{550} = 0.27.

Results of these case studies highlight how the water reflectance accuracy decreases for higher aerosol loading, particularly, when the atmospheric correction is

AMTD
7, 5147–5172, 2014

performed by using the urban aerosol in the HICO@CRI algorithm. The water reflectance is mainly correlated for the AERONET inversion products and the maritime type, independently from the luminosity of the ROIs, like attested by Fig. 6. This is observed also for the 4 May 2011 case, although the water reflectance obtained from the HICO@CRI with AERONET inversion products for the ROIrL shows negative values. Furthermore, the tri-modal size distribution observed on 4 May 2011 could be related to the spike shown in the Fig. 6 for $\tau_{550} = 0.08$. This result suggests that the sensitivity of the 6SV to a tri-modal size distribution needs to be investigated more in depth when atmospheric correction of hyperspectral data over water surface is performed.

Finally, errors on the retrieved water reflectance are greater for the continental and urban aerosol types than for maritime one.

6 Discussion and conclusions

The study shows the impact of different aerosol types on the results of the physically-based atmospheric correction of hyperspectral data characterized by low reflectance. To this aim, the HICO@CRI (HICO™ ATmospherically Corrected Reflectance Image) atmospheric correction algorithm was developed and applied to HICO™ images acquired on the northern Mediterranean Basin, when the inversion products of the AAOT (Acqua Alta Oceanographic Tower) site were available. The aerosol loading defined by the aerosol optical thickness at 550 nm, τ_{550}, and the columnar content of the water vapor, wvcc, and ozone, occ, were constrained to the values downloaded from the AAOT site. The analysis has been performed for the HICO™ images acquired for different values of the aerosol loading ($\tau_{550} < 0.3$) and with clear-sky condition. A measured aerosol, described by size distribution and refractive index, obtained at AAOT station was used as benchmark to evaluate the accuracy of the water reflectance obtained from the atmospheric correction performed using the maritime, continental and urban 6SV default aerosol types. Results show that the accuracy of the retrieved water

AMTD
7, 5147–5172, 2014

reflectance depends on the aerosol type used in the atmospheric correction processing, in addition to the influence of aerosol loading.

The Normalized Root Mean Square Error (NRMSE) attests the decrease of the retrieved water reflectance accuracy with growing aerosol loading. The accuracy of the atmospheric correction results depends on the τ_{550} and also on the aerosol type, mainly if the aerosol loading is non negligible.

In the case study, the AERONET micro-physical properties suggest that the aerosol type during the HICO™ acquisition is comparable to the maritime 6SV default aerosol type. The NRMSE increases if an unsuitable aerosol type is considered during the atmospheric correction, principally if the aerosol is composed by basic components with non negligible absorption, like the urban type. Thus, the improvement of the water reflectance retrieval requires more attention on the aerosol type during the atmospheric correction processing. The presence of absorbing aerosol leads to a significant contribution of the absorption on the radiative simulation of the solar radiation extinction and, consequently, in the water reflectance obtained from the Eqs. (1) and (2). The absorption of the urban type is non negligible; consequently the extinction is not dominated by the scattering, like for the maritime and continental types. This situation is confirmed by the optical properties of the urban aerosol presented in the Fig. 2.

Results of this work highlight the dependence of the atmospheric correction of water surface on the aerosol type. The sensitivity to the aerosol type derives from the components of the radiative field in the Eqs. (1) and (2), simulated for specific values of micro-physical and optical properties of the aerosol, by using the 6SV radiative transfer code (Kotchenova et al., 2008). During the HICO™ acquisition considered in this study, the Northern Mediterranean Basin was characterized with maritime aerosol, whereas the continental and urban types seem to be not consistent with the AERONET inversion products and to lead to inaccurate atmospheric correction results.

Consequently, the radiative impact of the aerosol type is not negligible when the atmospheric correction of hyperspectral data over coastal environment is performed. The retrieved water reflectance is sensitive to the aerosol type and the suitable aerosol

AMTD
7, 5147–5172, 2014

type has to be chosen to avoid errors on the water reflectance evaluation. The results of this work might be useful for applying atmospheric correction algorithms to remote sensing data used in water quality applications.

Acknowledgements. This work was undertaken as part of the CLAM-PHYM Project, funded by the Italian Space Agency (ASI, contract No. I/015/11/0). We are grateful to G. Zibordi for his valuable comments and for providing data of the AAOT station belonging to the AERONET and AERONET-OC networks. The HICO™ images used for this study were provided by the Naval Research Laboratory, USA and the Oregon State University within the project "Using HICO™ data for the preparation of the incoming Italian satellite hyperspectral mission PRISMA". Thanks are due to A. Pietrodangelo and to S. Schmidt for their supporting revising this manuscript.

References

Arabas, S., Schellens, M., Coulais, A., Gales, J., and Messmer, P.: GNU data language (GDL) – a free and open-source implementation of IDL, Geophys. Res. Abstr., EGU2010-924-1, EGU General Assembly 2010, Vienna, Austria, 2010. 5153

Bassani, C., Cavalli, R. M., and Pignatti, S.: Aerosol optical retrieval and surface reflectance from airborne remote sensing data over land, Sensors, 10, 6421–6438, doi:10.3390/s100706421, 2010. 5148, 5153, 5154

Bassani, C., Cavalli, R. M., and Antonelli, P.: Influence of aerosol and surface reflectance variability on hyperspectral observed radiance, Atmos. Meas. Tech., 5, 1193–1203, doi:10.5194/amt-5-1193-2012, 2012. 5149

Brando, V. and Dekker, A.: Satellite hyperspectral remote sensing for estimating estuarine and coastal water quality, IEEE T. Geosci. Remote, 41, 1378–1387, doi:10.1109/TGRS.2003.812907, 2003. 5152

Coulais, A., Schellens, M., Gales, J., Arabas, S., Boquien, M., Chanial, P., Messmer, P., and Fillmore, D.: Status of GDL – GNU Data Language, in: Astronomical Data Analysis Software and Systems XIX, Vol. 434 of ASP Conference Series, Springer, Sapporo, Japan, 2009. 5153

d'Almeida, G. A., Koepke, P., and Shettle, E. P.: Atmospheric Aerosols: Global Climatology and Radiative Characteristics, A. Deepak Publishing, Hampton, Virginia, USA, 1991. 5152, 5166

AMTD
7, 5147–5172, 2014

Gao, B.-C., Montes, M. J., Davis, C. O., and Goetz, A. F. H.: Atmospheric correction algorithms for hyperspectral remote sensing data of land and ocean, Remote Sens. Environ., 113, S17–S24, doi:10.1016/j.rse.2007.12.015, 2009. 5149

Giardino, C., Bresciani, M., Pilkaitytė, R., Bartoli, M., and Razinkovas, A.: In situ measurements and satellite remote sensing of case 2 waters: first results from the Curonian Lagoon, Oceanologia, 52, 197–210, doi:10.5697/oc.52-2.197, 2010. 5152

Goetz, A. F. H., Vane, G., Salomon, J. E., and Rock, B. N.: Imaging spectroscopy for Earth remote sensing, Science, 228, 1147–1153, doi:10.1126/science.228.4704.1147, 1985. 5149

Guanter, L., Alonso, L., and Moreno, J.: A method for the surface reflectance retrieval from PROBA/CHRIS data over land: application to ESA SPARC campaigns, IEEE T. Geosci. Remote, 43, 2908–2917, doi:10.1109/TGRS.2005.857915, 2005. 5149

Guanter, L., Estellés, V., and Moreno, J.: Spectral calibration and atmospheric correction of ultra-fine spectral and spatial resolution remote sensing data, application to CASI-1500 data, Remote Sens. Environ., 109, 54–65, doi:10.1016/j.rse.2006.12.005, 2007. 5149, 5154

Guanter, L., Richter, R., and Kaufmann, H.: On the application of the MODTRAN4 atmospheric radiative transfer code to optical remote sensing, Int. J. Remote Sens., 30, 1407–1424, doi:10.1080/01431160802438555, 2009a. 5154

Guanter, L., Segl, K., and Kaufmann, H.: Simulation of optical remote-sensing scenes with application to the EnMAP hyperspectral mission, IEEE T. Geosci. Remote, 47, 2340–2351, doi:10.1109/TGRS.2008.2011616, 2009b. 5149

Guanter, L., Ruiz-Verdú, A., Odermatt, D., Giardino, C., Simis, S., Estellés, V., Heege, T., Domínguez-Gómez, J. A., and Moreno, J.: Atmospheric correction of ENVISAT/MERIS data over inland waters: validation for European lakes, Remote Sens. Environ., 114, 467–480, doi:10.1016/j.rse.2009.10.004, 2010. 5152

Holben, B., Eck, T., Slutsker, I., Tanré, D., Buis, J., Setzer, A., Vermote, E., Reagan, J., Kaufman, Y., Nakajima, T., Lavenu, F., Jankowiak, I., and Smirnov, A.: AERONET – a federated instrument network and data archive for aerosol characterization, Remote Sens. Environ., 66, 1–16, doi:10.1016/S0034-4257(98)00031-5, 1998. 5148, 5149, 5150

Kaufman, Y. J., Tanré, D., Remer, L. A., Vermote, E. F., Chu, A., and Holben, B. N.: Operational remote sensing of tropospheric aerosol over land from EOS moderate resolution imaging spectroradiometer, J. Geophys. Res., 102, 17051–17067, doi:10.1029/96JD03988, 1997a. 5148, 5149, 5155

AMTD
7, 5147–5172, 2014

Kaufman, Y. J., Wald, A., Remer, L. A., Gao, B.-C., Li, R. R., and Flynn, L.: The MODIS 2.1 µm channel – correlation with visible reflectance for use in remote sensing of aerosol, IEEE T. Geosci. Remote, 35, 1286–1298, doi:10.1109/36.628795, 1997b. 5148

Kaufman, Y. J., Gobron, N., Pinty, B., Widlowski, J.-L., and Verstraete, M. M.: Relationship between surface reflectance in the visible and mid-IR used in MODIS aerosol algorithm – theory, Geophys. Res. Lett., 29, 31-1–31-4, doi:10.1029/2001GL014492, 2002. 5149

King, M., Kaufman, Y., Tanré, D., and T. Nakajima, T.: Remote sensing of tropospheric aerosols from space: past, present, and future, B. Am. Meteorol. Soc., 88, 2229–2259, doi:10.1175/1520-0477(1999)080<2229:RSOTAF>2.0.CO;2, 1999. 5148

Kokhanovsky, A. A.: Aerosol optics: light absorption and scattering by particles in the atmosphere, Praxis Publishing Ltd, Chichester, UK, 2008. 5148, 5152, 5153, 5166

Kokhanovsky, A. A., Breon, F.-M., Cacciari, A., Carboni, E., Diner, D., Nicolantonio, W. D., Grainger, R. G., Grey, W. M. F., Höller, R., Lee, K.-H., Li, Z., North, P. R. J., Sayer, A. M., Thomas, G. E., and von Hoyningen-Huene, W.: Aerosol remote sensing over land: a comparison of satellite retrievals using different algorithms and instruments, Atmos. Res., 85, 372–394, doi:10.1016/j.atmosres.2007.02.008, 2007. 5148

Kokhanovsky, A. A., Deuzé, J. L., Diner, D. J., Dubovik, O., Ducos, F., Emde, C., Garay, M. J., Grainger, R. G., Heckel, A., Herman, M., Katsev, I. L., Keller, J., Levy, R., North, P. R. J., Prikhach, A. S., Rozanov, V. V., Sayer, A. M., Ota, Y., Tanré, D., Thomas, G. E., and Zege, E. P.: The inter-comparison of major satellite aerosol retrieval algorithms using simulated intensity and polarization characteristics of reflected light, Atmos. Meas. Tech., 3, 909–932, doi:10.5194/amt-3-909-2010, 2010. 5148

Kotchenova, S. Y., Vermote, E. F., Levy, R., and Lyapustin, A.: Radiative transfer codes for atmospheric correction and aerosol retrieval: intercomparison study, Appl. Optics, 47, 2215–2226, doi:10.1364/AO.47.002215, 2008. 5149, 5153, 5154, 5159

Lenoble, J.: Radiative Transfer in Scattering and Absorbing Atmospheres: Standard Computational Procedures, A. Deepak Publishing, Hampton, Virginia, USA, 1985. 5152, 5166

Levy, R. C., Remer, L. A., and Dubovik, O.: Global aerosol optical properties and application to Moderate Resolution Imaging Spectroradiometer aerosol retrieval over land, J. Geophys. Res., 112, D13210, doi:10.1029/2006JD007815, 2007. 5148

Lucke, R. L., Corson, M., McGlothlin, N. R., Butcher, S. D., Wood, D. L., Korwan, D. R., Li, R. R., Snyder, W. A., Davis, C. O., and Chen, D. T.: Hyperspectral imager for the

AMTD
7, 5147–5172, 2014

coastal ocean: instrument description and first images, Appl. Optics, 50, 1501–1516, doi:10.1364/AO.50.001501, 2011. 5150, 5151

Mélin, F., Clerici, M., Zibordi, G., and Bulgarelli, B.: Aerosol variability in the Adriatic Sea from automated optical field measurements and Sea-viewing Wide Fiel-of-view Sensor (SeaWiFS), J. Geophys. Res., 111, D22201, doi:10.1029/2006JD007226, 2006. 5149, 5150, 5151, 5152

Moses, W. J., Bowles, J. H., Lucke, R. L., and Corson, M. R.: Impact of signal-to-noise ratio in a hyperspectral sensor on the accuracy of biophysical parameter estimation in case II waters, Opt. Express, 20, 4309–4330, doi:10.1364/OE.20.004309, 2012. 5156

Smirnov, A., Holben, B., Slutsker, I., Giles, D., McClain, C., Eck, T., Sakerin, S., Macke, A., Croot, P., Zibordi, G., Quinn, P., Sciare, J., Kinne, S., Harvey, M., Smyth, T., Piketh, S., Zielinski, T., Proshutinsky, A., Goes, J., Nelson, N., Larouche, P., Radionov, V., Goloub, P., Moorthy, K. K., Matarrese, R., Robertson, E., and Jourdin, F.: Maritime Aerosol Network as a component of Aerosol Robotic Network, J. Geophys. Res., 114, D06204, doi:10.1029/2008JD011257, 2009. 5150

Smirnov, A., Holben, B. N., Giles, D. M., Slutsker, I., O'Neill, N. T., Eck, T. F., Macke, A., Croot, P., Courcoux, Y., Sakerin, S. M., Smyth, T. J., Zielinski, T., Zibordi, G., Goes, J. I., Harvey, M. J., Quinn, P. K., Nelson, N. B., Radionov, V. F., Duarte, C. M., Losno, R., Sciare, J., Voss, K. J., Kinne, S., Nalli, N. R., Joseph, E., Krishna Moorthy, K., Covert, D. S., Gulev, S. K., Milinevsky, G., Larouche, P., Belanger, S., Horne, E., Chin, M., Remer, L. A., Kahn, R. A., Reid, J. S., Schulz, M., Heald, C. L., Zhang, J., Lapina, K., Kleidman, R. G., Griesfeller, J., Gaitley, B. J., Tan, Q., and Diehl, T. L.: Maritime aerosol network as a component of AERONET – first results and comparison with global aerosol models and satellite retrievals, Atmos. Meas. Tech., 4, 583–597, doi:10.5194/amt-4-583-2011, 2011. 5150

Tanré, D., Kaufman, Y. J., Herman, M., and Mattoo, S.: Remote sensing of aerosol properties over oceans using the MODIS/EOS spectral radiances, J. Geophys. Res.-Atmos., 102, 16971–16988, doi:10.1029/96JD03437, 1997. 5149

Vermote, E. F. and Kotchenova, S.: Atmospheric correction for the monitoring of land surfaces, J. Geophys. Res.-Atmos., 113, D23S90, doi:10.1029/2007JD009662, 2008. 5149

Vermote, E. F., Saleous, N. E., Justice, C., Kaufman, Y., Privette, J., Remer, L., Roger, J., and Tanré, D.: Atmospheric correction of visible to middle-infrared EOS-MODIS data over land surfaces: background, operational algorithm and validation, J. Geophys. Res., 102, 675–686, doi:10.1029/97JD00201, 1997a. 5154

AMTD
7, 5147–5172, 2014

Vermote, E. F., Tanré, D., Deuzé, J. L., Herman, M., and Morcrette, J. J.: Second simulation of the satellite signal in the solar spectrum, 6S: an overview, IEEE T. Geosci. Remote, 35, 675–686, doi:10.1109/36.581987, 1997b. 5149, 5153, 5154

Vermote, E. F., Tanré, D., Deuzé, J. L., Herman, M., Morcrette, J. J., and Kotchenova, S. Y.: Second Simulation of a Satellite Signal in the Solar Spectrum-Vector (6SV), available at: http://6s.ltdri.org (last access: 23 May 2014), 6S User Guide Version 3, 2006. 5149, 5152, 5155, 5166

Zibordi, G., Mélin, F., Berthon, J.-F., Holben, B., Slutsker, I., Giles, D., D'Alimonte, D., Vandemark, D., Feng, H., Schuster, G., Fabbri, B. E., Kaitala, S., and Seppälä, J.: AERONET-OC: a network for the validation of ocean color primary products, J. Atmos. Ocean. Tech., 26, 1634–1651, doi:10.1175/2009JTECHO654.1, 2009. 5150

Zibordi, G., Berthon, J.-F., Mélin, F., and D'Alimonte, D.: Cross-site consistent in situ measurements for satellite ocean color applications: the BiOMaP radiometric dataset, Remote Sens. Environ., 115, 2104–2115, doi:10.1016/j.rse.2011.04.013, 2011. 5152

AMTD
7, 5147–5172, 2014

Table 1. The simultaneous HICO™ and CIMEL acquisition with the τ_{550}, wvcc, occ and the Angstrom coefficient downloaded from the AAOT AERONET station. The selected images meet the clear-sky requirement.

Date (yyyy/mm/dd)	HICO™ (hh:mm)	CIMEL (hh:mm)	τ_{550}	Water Vapor (cm)	Ozone (Dobson)	Angstrom $\alpha_{470/870}$
2011/05/04	13:07	13:06	0.08 (lev2.0)	0.696 (lev2.0)	367.51 (lev2.0)	1.884 (lev2.0)
2012/01/11	13:21	13:18	0.05 (lev2.0)	0.949 (lev2.0)	326.23 (lev2.0)	1.769 (lev2.0)
2012/03/09	13:42	13:36	0.10 (lev2.0)	0.762 (lev2.0)	362.16 (lev2.0)	1.820 (lev2.0)
2012/05/12	7:18	7:20	0.25 (lev2.0)	2.381 (lev2.0)	364.15 (lev2.0)	1.599 (lev2.0)
2012/08/27	12:57	13:01	0.01 (lev2.0)	1.528 (lev2.0)	309.84 (lev2.0)	0.336 (lev2.0)
2013/04/25	13:03	13:08	0.27 (lev1.5)	1.969 (lev1.5)	371.40 (lev1.5)	0.851 (lev2.0)

AMTD
7, 5147–5172, 2014

Table 2. The volumetric percentage of the four basic components (sea-salt, water-soluble, soot and dust-like) describing the optical behavior of maritime, continental, and urban aerosol type, (Lenoble, 1985; d'Almeida et al., 1991; Vermote et al., 2006; Kokhanovsky, 2008).

	Water-soluble	Soot	Dust-like	Oceanic
Maritime	5 %			95 %
Continental	29 %	1 %	70 %	
Urban	61 %	22 %	17 %	

AMTD
7, 5147–5172, 2014

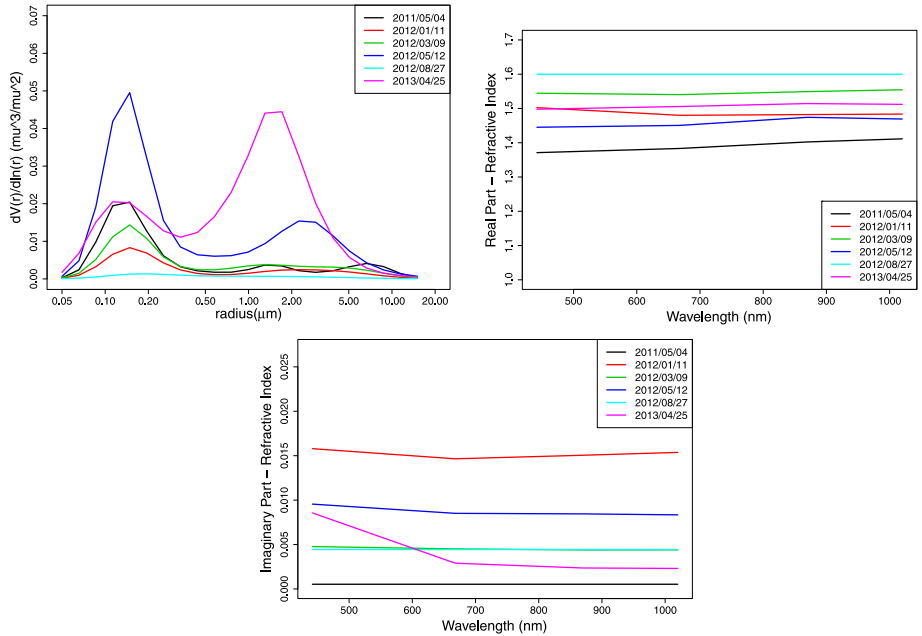

Figure 1. An example of the micro-physical properties of the aerosol downloaded from the AERONET AAOT station. The micro-physical properties values are the size distribution (on the left), the real part of the refractive index (on the centre), and the imaginary part (on the right), of the CIMEL acquisition.

AMTD
7, 5147–5172, 2014

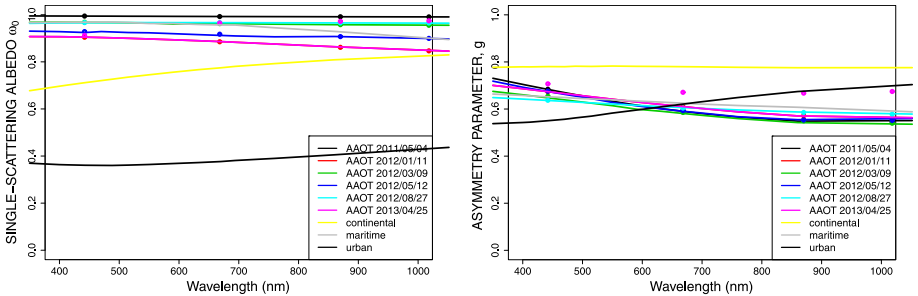

Figure 2. The single-scattering albedo and the asymmetry factor of the maritime, continental, and urban aerosol type (continous lines) and the AERONET inversion products (dots) in the 400–900 nm spectral domain for the HICO™ images.

AMTD
7, 5147–5172, 2014

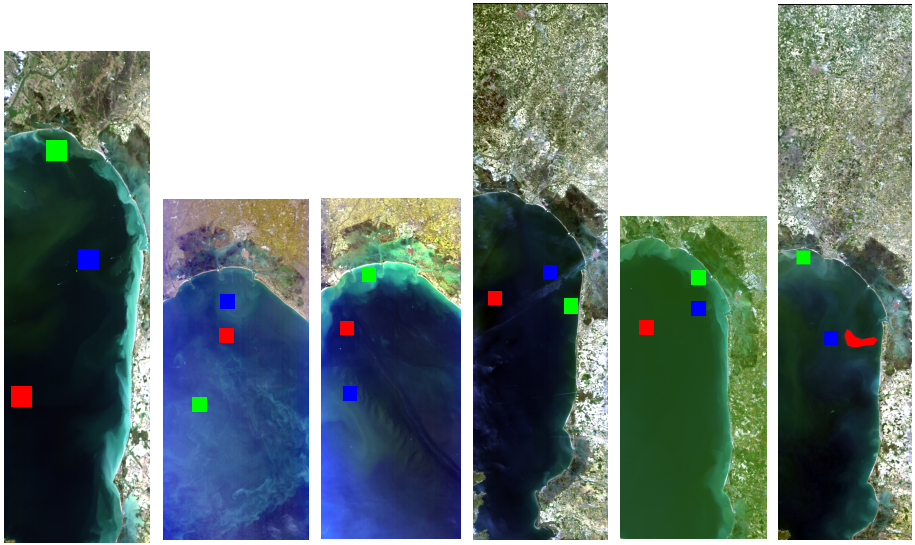

Figure 3. The available HICO™ images (using channel 11, 462 nm, for blue; 26, 548 nm, for green; 43, 645 nm, for red) show the three Regions Of Interest (ROIs) chosen to evaluate the contribution of the aerosol types over different kind of water in the six available HICO™ images. The red is for the low, the blue for the medium and the green for the high luminosity of the water body.

AMTD
7, 5147–5172, 2014

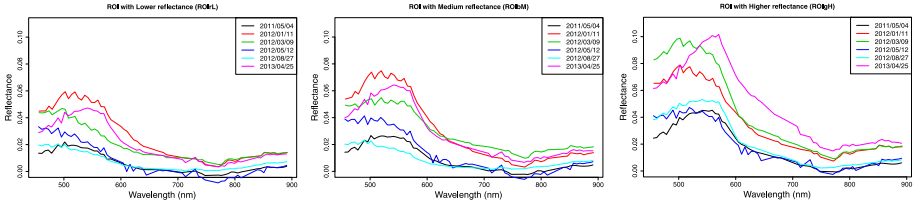

Figure 4. The mean water reflectance calculated in the ROIs of the used HICO images obtained applying HICO@CRI algorithm with the AERONET inversion products provided by AAOT station.

AMTD
7, 5147–5172, 2014

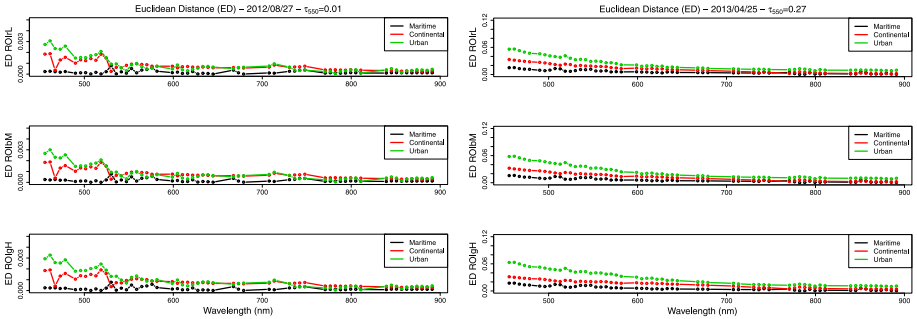

Figure 5. The Euclidean Distance (ED) between the mean water reflectance calculated in the ROIs (ROIrL, ROIbM, ROIgH) with the aerosol types implemented in the 6SV and the CIMEL inversion products. On the right, the ED calculated for the HICO image acquired the 27 August 2012 with $\tau_{550} = 0.01$ and on the left, the image acquired the 25 April 2013 with $\tau_{550} = 0.27$.

AMTD
7, 5147–5172, 2014

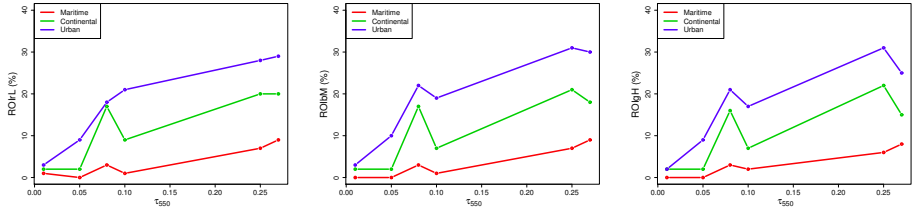

Figure 6. The Normalized Root Mean Square of the water reflectance retrieved with the aerosol types (urban, continental, and maritime) respect to the AERONET inversion products, calculated for the ROIs. Starting from the left, the calculation for the low, medium and high reflectance water types.

AMTD
7, 5147–5172, 2014